Electromagnetic Fields and Power Deposition in Body-of-Revolution Models of Man

TE-KAO WU, MEMBER, IEEE

Abstract—**Internal electromagnetic (EM) fields and power absorption in a homogeneous lossy dielectric body of revolution are evaluated using the surface integral equation method. The method yields moment method solutions for the induced current densities on the body surface. The interior fields to the body are then evaluated via the reciprocity theorem and the measurement matrix concept. The bulk body power deposition is obtained by the integration of the surface Poynting vector. The method applies for a wide range of dielectric parameters (with ϵ_r from 1.1 to 10^2 and σ from 0 to 10^3 mhos/m) in the resonance region. Numerical results for EM fields and power deposition in a body-of-revolution model of a human torso with height of 1.78 m are evaluated for frequencies of 30, 80, and 300 MHz. It is found that the strongest power deposition in the torso model occurs for fields polarized along the longest dimension and for frequencies near the first resonance (i.e., 80 MHz) of the torso body. Hot spots are also observed in the neck region of the torso body.**

I. Introduction

LIVING in today's electromagnetic (EM) wave bombarded environment, scientists have become concerned about the problem of possible biological hazards of microwave radiation. In the past, many analytical works have been presented to investigate the EM power absorption patterns and total absorption in simple three-dimensional models of man, e.g., spheres [1], spheroids [2], [3], and ellipsoids [4]. It was found that the power absorption characteristics are dependent on the frequency and orientation of those models with respect to the EM wave-field vectors. For realistic models with arbitrary contours, the integral equation method should prove to be advantageous. Recently, a volume integral equation (VIE) method has been developed by Livesay, Chen, and Guru [5], [6] to evaluate the internal fields and absorbed power density in finite slabs and thin cylinders of biological tissue as well as human torso models made of small cubical blocks. Some interesting hot spots were found in the neck or groin region of their models when it is illuminated by an EM wave with a frequency in the resonance region. The experimental work by Gandhi [7] also shows hot spots in the neck and thigh regions.

To detect these hot spots, a surface integral equation (SIE) method involving integrals of induced currents on the interface between air and the biological body of revolution is developed in this paper. The SIE method has been previously used by Wu and Tsai [8] to evaluate the EM fields induced inside arbitrarily shaped biological cylinders. There it has been shown that the SIE method is more advantageous than the VIE method in treating larger sized homogeneous dielectric bodies. The SIE method has also been successfully used to calculate the EM scattering by an inhomogeneous dielectric cylinder of biological tissue by using an invariant imbedding technique [9]. The feasibility of using the SIE method to evaluate the induced surface currents and far-field patterns of a homogeneous biological body of revolution has also been demonstrated in a recent paper [10]. Therefore, the interior fields to the biological body are now obtained from the previously calculated surface currents, the reciprocity theorem, and the measurement matrix concept. By energy conservation principles, the time-averaged Poynting vectors of the total surface fields are also integrated to yield the total power deposition of the body.

To test the validity of this method, SIE solutions for the interior fields and power absorption of a homogeneous lossy dielectric sphere are compared with the exact solutions. Numerical results for the internal EM fields and power deposition in a body-of-revolution model of a human torso are next given to determine the power dependence on the frequency and polarization of the incident plane wave and to detect the so-called "hot spots."

II. Method of Solution

Fig. 1 shows the geometry of a homogeneous lossy dielectric body of revolution with ϵ_r and σ as the dielectric constant and conductivity, respectively. The solution method for determining the induced surface currents $\boldsymbol{J}$ (electric current density) and $\boldsymbol{K}$ (magnetic current density) has been presented in [10] when the body is illuminated by an incident plane wave. Thus in this section we will outline the SIE solutions for $\boldsymbol{J}$ and $\boldsymbol{K}$ and develop the formulas for computing the internal fields and the power deposition. The notation is that used in [10].

Starting from Maxwell's equation, Green's theorem, and the boundary conditions, one may easily formulate the following matrix equation [10]:

$$\begin{bmatrix} L_{11} & -L_{12} \\ L_{12} & L_{22} \end{bmatrix} \begin{bmatrix} \boldsymbol{J}_s \\ \boldsymbol{K}_s \end{bmatrix} = \begin{bmatrix} \boldsymbol{E}^i \\ \boldsymbol{H}^i \end{bmatrix} \tag{1}$$

where L_{11}, L_{12}, and L_{22} are integrodifferential operators given in [10]. $\boldsymbol{J}_s$ and $\boldsymbol{K}_s$ are the unknown electric and magnetic current densities on S, and $\boldsymbol{E}^i$ and $\boldsymbol{H}^i$ are the

Manuscript received August 14, 1978; revised October 30, 1978.

The author was with the Department of Electrical Engineering, University of Mississippi, University, MS 38677. He is now with Lockheed Missiles and Space Company, Inc., Sunnyvale, CA 94086.

0018-9480/79/0300-0279$00.75 ©1979 IEEE

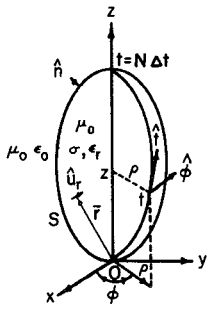

Fig. 1. Geometry and coordinate system of a body of revolution.

electric and magnetic fields of the incident plane wave. Notice that the above equation is implicitly valid for tangential components only. Since the body is rotationally symmetric about the z axis as shown in Fig. 1, the induced current densities can be represented by

$$\begin{cases} \boldsymbol{J}_s = \sum_{m=-M}^{M} \sum_{i=1}^{N} \left(a_{mi}\boldsymbol{J}_{mi}^{t} + b_{mi}\boldsymbol{J}_{mi}^{\phi}\right) \\ \boldsymbol{K}_s = \sum_{m} \sum_{i} \left(c_{mi}\boldsymbol{K}_{mi}^{t} + d_{mi}\boldsymbol{K}_{mi}^{\phi}\right) \end{cases} \tag{2}$$

where a_{mi}, b_{mi}, c_{mi}, and d_{mi} are constants to be determined and $\boldsymbol{J}_{mi}^{t}$, $\boldsymbol{J}_{mi}^{\phi}$, $\boldsymbol{K}_{mi}^{t}$, and $\boldsymbol{K}_{mi}^{\phi}$ are expansion functions of the type

$$\begin{cases} \boldsymbol{J}_{mi}^{t} = \boldsymbol{K}_{mi}^{t} = \hat{t} f_i(t) \exp(jm\phi) \\ \boldsymbol{J}_{mi}^{\phi} = \boldsymbol{K}_{mi}^{\phi} = \hat{\phi} f_i(t) \exp(jm\phi) \end{cases} \tag{3}$$

where the ϕ-expansion is a Fourier series in ϕ, $\hat{t}$ and $\hat{\phi}$ are the unit vectors of the orthogonal coordinate system (t,ϕ) for a point on S, and $f_i(t)$ is a triangular function divided by the distance ρ from the z axis. Allow next the testing functions to be

$$\begin{cases} \boldsymbol{W}_{mi}^{t} = \hat{t} f_i(t) \exp(-jm\phi) \\ \boldsymbol{W}_{mi}^{\phi} = \hat{\phi} f_i(t) \exp(-jm\phi) \end{cases} \tag{4}$$

and the inner product of two vectors $\boldsymbol{A}$ and $\boldsymbol{B}$ to be

$$\langle \boldsymbol{A}, \boldsymbol{B} \rangle = \int_S \boldsymbol{A} \cdot \boldsymbol{B} dS. \tag{5}$$

After testing each side of (1) with $\boldsymbol{W}_{mi}$, the constants a_{mi}, b_{mi}, c_{mi}, and d_{mi} are readily obtained from

$$[Z][I] = [V] \tag{6}$$

where $[Z]$ and $[V]$ are the generalized impedance and voltage matrices as given by [10, (12) and (10)], and

$$[I] = \left[[a_{mi}][b_{mi}][c_{mi}][d_{mi}] \right]^T \tag{7}$$

where T means transpose. The details for evaluating the above matrix elements can be found in [10].

To further evaluate the fields interior to the body, one may consider a current element $Il\hat{u}_r$ at $\boldsymbol{r}$, as shown in Fig. 1. From the reciprocity theorem [10]–[13], the electric field $\boldsymbol{E}(\boldsymbol{r})$ everywhere interior to S is determined by

$$\boldsymbol{u}_r \cdot \boldsymbol{E}(r) = \frac{1}{Il} \int_S \left[\boldsymbol{E}^d \cdot \boldsymbol{J}_s - \boldsymbol{H}^d \cdot \boldsymbol{K}_s \right] dS' \tag{8}$$

where $\boldsymbol{E}^d$ and $\boldsymbol{H}^d$ are the dipole fields of the current element $Il\hat{u}_r$ and are given by

$$\begin{cases} \boldsymbol{E}^d = -j\omega \boldsymbol{A} - \nabla\psi \\ \boldsymbol{H}^d = \dfrac{1}{\mu_0} \nabla \times \boldsymbol{A} \end{cases} \tag{9}$$

where $\boldsymbol{A}$ and ψ are the vector and scalar potentials

$$\boldsymbol{A} = \hat{u}_r \mu_0 Il \Phi_2 = \hat{u}_r \frac{\mu_0 Il}{4\pi} \frac{\exp(-jk|\boldsymbol{r}-\boldsymbol{r}'|)}{|\boldsymbol{r}-\boldsymbol{r}'|} \tag{10}$$

$$\psi = \frac{j}{\omega \epsilon_2} \nabla \cdot \boldsymbol{A} \tag{11}$$

$$\epsilon_2 = \epsilon_r \epsilon_0 - j\sigma/\omega \tag{12}$$

and

$$k = k_0(\epsilon_2/\epsilon_0)^{1/2}, \quad k_0 = 2\pi/\lambda_0, \quad \Phi_2 = \frac{\exp(-jk|\boldsymbol{r}-\boldsymbol{r}'|)}{4\pi|\boldsymbol{r}-\boldsymbol{r}'|}. \tag{13}$$

Equation (8) may be rewritten in terms of the measurement matrix similar to that in [12], i.e.,

$$\hat{u}_r \cdot E(\boldsymbol{r}) = \frac{1}{Il} \sum_{m=-M}^{M} [R_m][I_m] \exp(jm\phi) \tag{14}$$

where $[I_m]$ is obtained from (7), $[R_m]$ is the near-field measurement matrix and is given by

$$[R_m] = \left[[R_{mi}^{t}][R_{mi}^{\phi}][\bar{\boldsymbol{R}}_{mi}^{t}][\bar{\boldsymbol{R}}_{mi}^{\phi}] \right]. \tag{15}$$

The bracketed quantities on the right-hand side of (15) are two-dimensional surface integrals. For example:

$$\bar{\boldsymbol{R}}_{mi}^{t} = -Il \int dt'(\rho' f_i) \int d\phi' \left[\hat{t}' \cdot (\nabla' \Phi_2 \times \hat{u}_r) \right] \exp(jm\phi'). \tag{16}$$

To evaluate the above double integrals, similar approximations to those in [11] are used. That is, for the t' integration, four flat pulses are used to approximate the triangle basis function. Further approximation similar to that in [11, (46)–(55)] is used to eliminate the t' integral. For the ϕ' integral, the numerical integration scheme of Gaussian quadrature [14] is used.

The bulk body power deposition may now be computed via the energy conservation principle [15] as

$$P = -\mathrm{Re} \int_S (\boldsymbol{E} \times \boldsymbol{H}^*) \cdot \hat{n} dS \tag{17}$$

where $\boldsymbol{E} \times \boldsymbol{H}^*$ is the time-averaged Poynting vector of the total surface fields (i.e., the induced current densities $\boldsymbol{J}_s$ and $\boldsymbol{K}_s$). Thus in terms of the current coefficients of (2), (17) may be rewritten as

$$\begin{aligned} P &= -\mathrm{Re} \int_S (K^t J^{\phi *} - K^{\phi} J^{t *}) dS \\ &= -\mathrm{Re} \left[2\pi \sum_{m=-M}^{M} \sum_{i=1}^{N} (b_{mi}^* c_{mi} - d_{mi} a_{mi}^*) \int_0^{N\Delta t} \rho f_i^2(t) dt \right] \end{aligned} \tag{18}$$

where * denotes complex conjugate and Re (A) means the real part of the complex quantity A. Here the t integral may be evaluated using the two-point Gaussian quadrature integration routine.

The absorption efficiency Q_{abs} as defined in [3] is next calculated as

$$Q_{abs} = \frac{P}{AS_i} \tag{19}$$

where A is the geometric cross section of the body and S_i is the incident power density.

III. Numerical Results and Discussion

The accuracy and convergence rate of the SIE solution for the induced surface current densities $\boldsymbol{J}_s$ and $\boldsymbol{K}_s$ on a dielectric sphere has been studied in [10]. It is recognized that the convergence rate for the currents on a dielectric body [10] is apparently of the same order as that for a conducting body [11]. Once the surface currents are accurately determined, using the formulas developed in the previous section, one may readily estimate the total power deposition and fields everywhere interior to the body. Table I shows the absorption efficiency Q_{abs} of a lossy dielectric sphere (with radius "a" and complex permittivity ϵ_2) illuminated by an axially incident plane wave. Here $m = \pm 1$ and nine triangles, i.e., $N = 10$, are used for the current's expansions. The SIE solutions for Q_{abs} are in good agreement with the results obtained by the extended boundary condition method [3]. The interior fields along the z axis of a muscle sphere ($\epsilon_r = 60$, $\sigma = 1$ mho/m, $f = 300$ MHz, and $a = 0.2\lambda$) are plotted in Fig. 2, with a vertically polarized plane wave ($E_z^i = -1$ V/m) propagating in the $-x$ direction. Notice that no E_y component is induced along the symmetric axis (i.e., z axis) for this polarization. The absorbed power densities (i.e., $p = (\sigma/2)\boldsymbol{E}\cdot\boldsymbol{E}^* = (\sigma/2)(|E_x|^2 + |E_y|^2 + |E_z|^2)$) are next plotted along the x, y, and z axes as shown in Fig. 3. As can be seen, excellent agreement is obtained between the SIE and exact solutions, which is obtained using the standard separation of variables method [15]; thus the SIE solution can be considered valid. It is also interesting to note that due to the dielectric loss, the absorbed power density, as shown in Fig. 3, is reduced greatly from the surface to the center of the sphere and from front to back.

One of the main objectives of this study is to demonstrate the applicability of the SIE method in the evaluation of the power absorption dependence on the frequency and polarization of the EM waves and the detection of resonance effects and possible hot spots. Toward that end, the interior fields and the total power deposition in a body-of-revolution model of a human torso are evaluated for a vertically or horizontally polarized incident plane wave at three frequencies, i.e., 30, 80, and 300 MHz. Here the human torso is modeled by a homogeneous dielectric body of revolution of muscle tissue with a height of 1.78 m, as shown in Fig. 4. Figs. 4–6 show the magnitude of interior fields E_z and E_x along the z axis, with a vertically

TABLE I
Absorption Efficiency of Dielectric Spheres (with Radius "a" and Permittivity ϵ_2)

$k_0 a$ \ ϵ_2/ϵ_0	3.536(1-j)	7.071(1-j)	14.142(1-j)
0.5	0.448	0.4	0.465
1.0	1.09	1.24	1.09
1.5	1.14	1.1	0.894

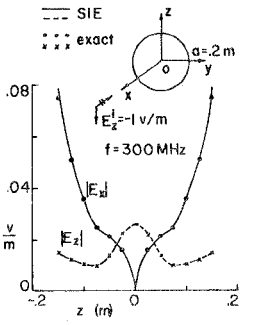

Fig. 2. Internal fields $|E_x|$ and $|E_z|$ along the z axis of a muscle sphere ($\epsilon_r = 60$, $\sigma = 1$ mho/m, $a = 0.2$ m, $f = 300$ MHz) with a vertically polarized plane wave ($E_z^i = -1$ V/m) propagating in the $-x$ direction ($m = 0, \pm 1$, and $N = 10$).

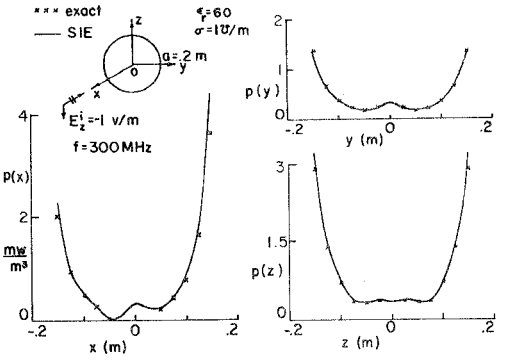

Fig. 3. Absorbed power densities along the x, y, and z axes of the same muscle sphere as in Fig. 2, vertical polarization ($m = 0, \pm 1, \pm 2, \pm 3$, and $N = 10$).

polarized plane wave (i.e., $E_z^i = -1$ V/m) propagating in the $-x$ direction for frequency at 300, 80, and 30 MHz, respectively. Similar to the sphere case, no E_y component is induced along the z axis. The absorbed power density can be easily determined by the sum "$(\sigma/2)(|E_x|^2 + |E_z|^2)$." Note that the z axis is chosen to be the symmetry axis and aligned with the longest dimension of the torso model. As can be seen, the strongest induced electrical field occurs at 80 MHz, since at this frequency the torso model exhibits the first resonance phenomenon in response to the vertically polarized plane wave. Hot spots are also found in the neck region for all three frequencies.

In the case of a horizontally polarized plane wave (i.e., $E_y^i = 1$V/m) illuminating the same torso in the $-x$ direction, the interior fields $|E_y|$ along the z axis are much smaller than those of the vertical polarization case and are

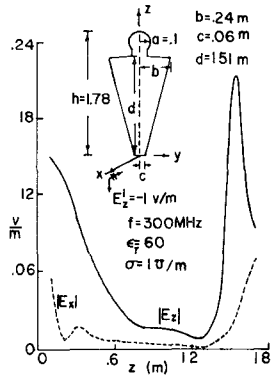

Fig. 4. Internal fields $|E_x|$ and $|E_z|$ along the z axis of a body-of-revolution model of man, vertical polarization, $f=300$ MHz ($m=0, \pm 1$, and $N=21$).

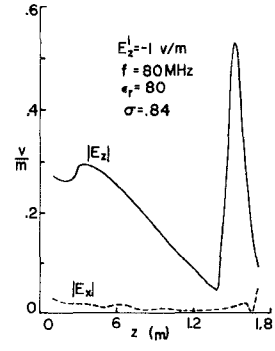

Fig. 5. Internal fields $|E_x|$ and $|E_z|$ along the z axis of the same torso model as in Fig. 4, vertical polarization, $f=80$ MHz ($m=0, \pm 1$, and $N=21$).

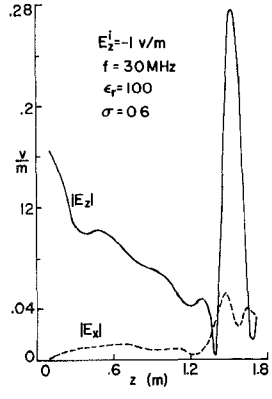

Fig. 6. Internal fields $|E_x|$ and $|E_z|$ along the z axis of the same torso model as in Fig. 4, vertical polarization, $f=30$ MHz ($m=0, \pm 1$, and $N=11$).

not shown here. Local hot spots for this horizontal polarization case are also found in the neck region. The total power deposition in this torso model with the vertical (i.e., $E_z^i=-1$ V/m) or horizontal (i.e., $E_y^i=1$ V/m) polarization are given in Table II. As was observed in other independent works [2], [6], [7], the strongest power deposition in the torso is found for the case of vertical polarization and for frequencies near the first resonance of the torso body. It should be noted that though only fields along the z axis are shown, fields elsewhere interior to the body may also be readily evaluated.

TABLE II
BULK BODY POWER DEPOSITION P (IN MILLIWATTS) IN THE TORSO MODEL
($m=0, \pm 1, \pm 2, \pm 3$)

freq. (in MHz) / polarization	30	80	300
vertical	0.271	2.557	0.544
Horizontal	0.051	0.053	0.472

IV. CONCLUDING REMARKS

In this paper, the feasibility of using the SIE technique to analyze the EM fields and power deposition in a homogeneous dielectric body of revolution of biological tissue has been demonstrated. The method also applies for any arbitrarily shaped body-of-revolution models of man and animals, e.g., human torsos, monkeys, rats, etc. Although the illuminating sources considered here are plane waves, for near zone sources such as manpack radio antennas [13], direct-contact aperture sources, corner reflectors, etc., this technique still applies.

If the internal EM fields vary both rapidly and drastically inside the biological body, some resonance peaks and nulls might be missed by using the VIE method because of its resolution limit. While using the SIE method, fields *everywhere* interior to the body are accurately evaluated. Furthermore, the SIE method may be generalized to analyze inhomogeneous bodies by employing the invariant imbedding technique [9], and the method applies for a wide range of dielectric parameters (with ϵ_r from 1.1 to 10^2 and σ from 0 to 10^3 mhos/m). In closing, because of the versatility of moment method solutions to changes in geometry, a myriad of body configurations may also become tractable, e.g., a human torso with outstretched arms and legs, or even carrying a manpack transceiver.

ACKNOWLEDGMENT

The author is indebted to the reviewer for a thorough reading of the manuscripts and many helpful suggestions.

REFERENCES

[1] J. C. Lin, A. W. Guy, and C. C. Johnson, "Power deposition in a spherical model of man exposed to 1–20 MHz electromagnetic field," *IEEE Trans. Microwave Theory Tech.*, vol. MTT-21, pp. 791–797, Dec. 1973.

[2] C. C. Johnson, C. H. Durney, and H. Massoudi, "Long-wavelength electromagnetic power absorption in prolate spheroid models of man and animals," *IEEE Trans. Microwave Theory Tech.*, vol. MTT-23, pp. 739–747, Sept. 1975.

[3] P. W. Barber, "Resonance electromagnetic absorption by nonspherical dielectric objects," *IEEE Trans. Microwave Theory Tech.*, vol. MTT-25, pp. 373–381, May 1977.

[4] H. Massoudi, C. H. Durney, and C. C. Johnson, "Long-wavelength power absorption in ellipsoidal models of man and animals," *IEEE Trans. Microwave Theory Tech.*, vol. MTT-25, pp. 47–52, Jan. 1977.

[5] D. E. Livesay and K. M. Chen, "Electromagnetic fields induced

inside arbitrarily shaped biological bodies," *IEEE Trans. Microwave Theory Tech.*, vol. MTT-22, pp. 1273–1280, Dec. 1974.

[6] K. M. Chen and B. S. Guru, "Internal EM field and absorbed power density in human torsos induced by 1-500-MHz EM waves," *IEEE Trans. Microwave Theory Tech.*, vol. MTT-25, pp. 746–756, Sept. 1977.

[7] O. P. Gandhi, "Condition of strongest electromagnetic power deposition in man and animals," *IEEE Trans. Microwave Theory Tech.*, vol. MTT-23, pp. 1020–1029, Dec. 1975.

[8] T. K. Wu and L. L. Tsai, "Electromagnetic fields induced inside arbitrary cylinders of biological tissue," *IEEE Trans. Microwave Theory Tech.*, vol. MTT-25, pp. 61–65, Jan. 1977.

[9] R. J. Pogorzelski and T. K. Wu, "Computations of scattering from inhomogeneous penetrable elliptic cylinders by means of invariant imbedding," in *Proc. 1977 URSI Symp. on Electromagnetic Wave Theory* (Stanford University, June 20–24), pp. 323–325, 1977.

[10] T. K. Wu and L. L. Tsai, "Scattering from arbitrarily-shaped lossy dielectric bodies of revolution," *Radio Sci.*, vol. 12, no. 5, pp. 709–718, Sept.–Oct. 1977.

[11] J. R. Mautz and R. F. Harrington, "Radiation and scattering from bodies of revolution," *Appl. Sci. Res.*, vol. 20, pp. 405–435, June 1969.

[12] R. F. Harrington and J. R. Mautz, "Green's functions for surfaces of revolution," *Radio Sci.*, vol. 7, no. 5, pp. 603–611, May 1972.

[13] T. K. Wu and C. M. Butler, "Numerical Green's function for dielectric bodies of revolution and its applications," presented at the 1978 National Radio Science Meeting, Univ. of Colorado, Boulder, Jan. 1978.

[14] M. Abramowitz and T. Stegun, *Handbook of Mathematical Functions*. NBS, AMS-55, 1964, p. 887.

[15] R. F. Harrington, *Time-Harmonic Electromagnetic Fields*. New York: McGraw-Hill, 1961, pp. 20–22.